
Time-lapse rock physics CO₂ monitoring with FWI

Qi Hu and Kris Innanen

ABSTRACT

Carbon capture and storage is a viable greenhouse gas mitigation technology. Monitoring of the CO₂ storage process should, in addition to locating the plume, provide quantitative information on CO₂ saturation. We propose a full waveform inversion (FWI) algorithm for the prediction of the spatial distribution of CO₂ saturation from time-lapse seismic data. The methodology is based on the application of a rock-physics parameterized FWI scheme that allows for direct updating of reservoir properties. We derive porosity and lithology parameters from baseline data and use them as input to predict CO₂ saturation from monitor data. The method is tested on synthetic time-lapse data generated for the Johansen formation model. The results with realistic initial models and noisy data demonstrate the robustness of our approach for reconstructing baseline models. For the inversion of monitor data, we show that both the errors in baseline model estimates and the random noise could compromise the reconstructed CO₂ saturation model. We propose to improve the result using a regularization technique that consists of two penalty terms: the Tikhonov term to ensure smoothness and the prior model term to help the convergence towards expected models.

INTRODUCTION

One of the technologies to reduce greenhouse gas emissions is the geological storage of carbon dioxide (CO₂) as a sustainable and secure solution (Macquet et al., 2019). Suitable storage sites are for example depleted fossil fuel reservoirs and deep saline aquifers (Queißer and Singh, 2013a). Injection of CO₂ into brine-saturated reservoir rocks change their elastic moduli and thus changes the seismic response. Time-lapse seismic surveys, in which a series of seismic data sets are acquired at different times to study the temporal variation of a target subsurface area, can be used to monitor the migration and distribution of the CO₂ plume and warn leakage problem if any (Ghosh et al., 2015). For reliable conformance verification, the monitoring should also provide quantitative information on CO₂ saturation to be compared to reservoir modeling predictions (Dupuy et al., 2021).

Qualitative interpretation of CO₂ that is made by analyzing amplitude changes and time shifts on post-stack seismic images is often not sufficient to understand the detailed reservoir conditions (Alemie, 2017). Moreover, multiple reflections, interference effects such as tuning, and attenuation may render these seismic images ambiguous in terms of the localization of CO₂ (Queißer and Singh, 2013b). One alternative to address these issues consists in using full waveform inversion (FWI), which is a powerful method for obtaining high-resolution subsurface models by extracting the full information content of seismic data (Tarantola, 1986; Virieux and Operto, 2009; Brossier et al., 2009). The principle behind an inverse technique such as FWI is a straightforward means to account for all the aforementioned wave propagation effects. For time-lapse studies, FWI provides a convenient way to perform a comparison in the parameter space using models associated with different times. Moreover, the elastic parameters (e.g., velocity, density, and modulus) derived

from FWI can be directly linked to reservoir (or rock physics) properties, such as porosity, fluid saturation, and pore pressure. Therefore, FWI should appear as an attractive tool for quantitative CO₂ characterization and monitoring.

Progress has been reported in managing many of the challenges of practical FWI: its computational complexity, dependence on the starting model, sensitivity to incomplete data, etc. (Operto et al., 2013; Prioux et al., 2013; Métivier et al., 2017; Pan et al., 2019). Time-lapse FWI faces additional challenges in detecting small changes in the model, which can be easily obscured by various undesirable non-repeatability factors, such as ambient noise, near surface conditions, and source and receiver parameters (Kamei and Lumley, 2017). Efforts have been made to reduce the effects of such non-repeatability by the design of monitoring systems (Shulakova et al., 2015), data processing (Roach et al., 2015), and inversion strategies (Asnaashari et al., 2015; Alemie, 2017; Kamei and Lumley, 2017; Fu et al., 2020). As these occur, consideration of how to achieve full-wave extraction of reservoir changes, especially fluid saturation variations, becomes more relevant. The classical way of applying FWI in reservoir property estimation is to interpret the elastic parameters obtained from FWI in term of reservoir properties, a problem often referred to as rock physics inversion (Doyen, 2007; Grana, 2016). This interpretation requires a rock physics model that establishes a link between elastic and reservoir properties, and it is important that the rock physics model to be used is consistent with the local geology (Mavko et al., 2009). Nowadays, most efforts to involve FWI in CO₂ saturation prediction are of this sequential type. For example, Queißer and Singh (2013b) apply elastic FWI to the Sleipner time-lapse seismic data. They correlate velocity changes with CO₂ saturation changes using the Gassmann's equations. Also at Sleipner, Dupuy et al. (2021) combine acoustic FWI and rock physics inversion to estimate rock frame properties from baseline data and CO₂ saturation from monitor data.

A topic that is of active research is to estimate reservoir properties directly from the seismic data, as opposed to the sequential approach in which elastic parameters are estimated first, followed by reservoir properties. The direct approach essentially involves combination of wave propagation equations and rock physics model within an integrated formulation, guaranteeing consistency between elastic and reservoir properties (Doyen, 2007; Bosch et al., 2010). Most current workflows in this field are based on seismic amplitude variation with offset (AVO) and are carried out using stochastic algorithms (Bosch et al., 2007; Spikes et al., 2007; Grude et al., 2013; Liu and Grana, 2018; Grana et al., 2020). Compared to AVO inversion, FWI is capable of obtaining a superior subsurface model by going beyond the inherent assumptions of AVO and using wave equation solutions (Mallick and Adhikari, 2015). Some attempts are made to use poroelastic theory in FWI to directly relate seismic wave characteristics to porous media properties (De Barros and Dietrich, 2008; Morency et al., 2009; Yang et al., 2019). However, the inverse problem is highly under-determined and ill-posed, and the computational burden is very large (Dupuy et al., 2021). Recently, Hu et al. (2021) provide a novel approach to directly update rock and fluid properties using elastic FWI (i.e., EFWI). They achieve this by reparameterizing the inversion in terms of rock physics properties, adopting a viewpoint similar to that of Russell et al. (2011) within an AVO environment. The main advantages of this approach are: 1) it allows examination of any rock physics property that has a well-defined relationship with elastic parameters; 2) it leads to a more stable solution compared to the sequential inver-

sion; 3) it shares the same numerical structure as the conventional EFWI. Hu and Innanen (2021) further develop this approach by combining prior model information.

In this work, we propose to apply the method of Hu et al. (2021) to CO₂ saturation prediction from time-lapse seismic data. The rest of the paper is organized as follows. We first review the FWI framework of Hu et al. (2021) which allows for direct updates in rock physics properties. We illustrate how to use this approach in the time-lapse mode for quantitative CO₂ monitoring. We then demonstrate the effectiveness of the proposed method using synthetic time-lapse data generated from the Johansen model, offshore Norway. We propose to recover porosity and lithology parameters from baseline seismic data and then use their results as input in the monitor seismic survey to estimate CO₂ saturation. We should highlight how the errors in baseline model estimates and the errors in monitor data could compromise the reconstruction of CO₂ saturation. We also discuss inversion strategies for improving the CO₂ saturation prediction.

METHOD

Elastic FWI with rock-physics parameterizations

We consider isotropic elasticity and a 2D medium. In the frequency domain, the two-dimensional elastic wave equations can be written as (Pratt, 1990)

$$\begin{aligned}\omega^2 \rho u + \frac{\partial}{\partial x} \left[(\lambda + 2\mu) \frac{\partial u}{\partial x} + \lambda \frac{\partial v}{\partial z} \right] + \frac{\partial}{\partial z} \left[\mu \left(\frac{\partial u}{\partial z} + \frac{\partial v}{\partial x} \right) \right] + f &= 0, \\ \omega^2 \rho v + \frac{\partial}{\partial z} \left[(\lambda + 2\mu) \frac{\partial v}{\partial z} + \lambda \frac{\partial u}{\partial x} \right] + \frac{\partial}{\partial x} \left[\mu \left(\frac{\partial u}{\partial z} + \frac{\partial v}{\partial x} \right) \right] + g &= 0,\end{aligned}\tag{1}$$

where ω is the angular frequency, ρ is the density, u and v are, respectively, the horizontal and vertical displacements, f and g are the corresponding source terms, and λ and μ are the Lamé parameters. Equation 1 is discretized and solved using the finite difference equations, which take the form

$$\mathbf{A}\mathbf{u} = \mathbf{f},\tag{2}$$

where the coefficients of the impedance matrix \mathbf{A} depend on the frequency and the medium properties, $\mathbf{u} = (u, v)$ and $\mathbf{f} = (f, g)$. The coefficients within \mathbf{A} are determined by iteratively minimizing the differences between seismic observations \mathbf{d}_{obs} , and simulation of data \mathbf{d}_{syn} within model \mathbf{m} . The objective function to be minimized is

$$E(\mathbf{m}) = \frac{1}{2} \Delta \mathbf{d}^t \Delta \mathbf{d}^*,\tag{3}$$

where $\Delta \mathbf{d} = \mathbf{d}_{\text{obs}} - \mathbf{d}_{\text{syn}}$ contain the data residuals, and the superscripts t and * denote the transpose and the complex conjugate, respectively. The gradient of E with respect to the model parameter m is (Brossier et al., 2009)

$$\nabla_m E = \Re \left\{ \mathbf{u}^t \left(\frac{\partial \mathbf{A}}{\partial m} \right)^t (\mathbf{A}^{-1})^t \Delta \mathbf{d}^* \right\}.\tag{4}$$

where \Re takes the real part of its argument. The quantity $\partial \mathbf{A} / \partial m$ is the scattering radiation pattern associated with model unknown m . Within a Newton optimization, the search

direction $\delta\mathbf{m}$ for model update is the solution of

$$\mathbf{H} \delta\mathbf{m} = -\nabla_{\mathbf{m}}E, \quad (5)$$

where \mathbf{H} is the Hessian operator. We employ a truncated Gauss Newton method (Métivier et al., 2017), in which equation 6 is solved iteratively, involving only Hessian-vector products.

From equation 4 we observe that the model parameter is altered at each iteration by an update proportional to $\partial\mathbf{A}/m$. To formulate a model parameterization based on N different rock physics properties, at each node point we compute the chain rule

$$\frac{\partial\mathbf{A}}{\partial r_i} = \frac{\partial\mathbf{A}}{\partial e_1} \frac{\partial e_1}{\partial r_i} + \frac{\partial\mathbf{A}}{\partial e_2} \frac{\partial e_2}{\partial r_i} + \frac{\partial\mathbf{A}}{\partial e_3} \frac{\partial e_3}{\partial r_i}, \quad (6)$$

for each of $i = (1, 2, \dots, N)$, where $\mathbf{r} = (r_1, r_2, \dots, r_N)$ is the desired rock-physics parameterization; $\mathbf{e} = (e_1, e_2, e_3)$ is a conventional FWI parameterization based on three elastic properties, e.g., the P- and S-wave velocities plus density; Given a conventional FWI scheme set up to update parameters \mathbf{e} , within which the partial derivatives $\partial\mathbf{A}/e_j$ ($j = 1, 2, 3$) are known, and given the relations between \mathbf{e} and \mathbf{r} of the form $(e_1, e_2, e_3) = f(r_1, r_2, \dots, r_N)$, so that $\partial e_j/\partial r_i$ can be derived, through equation 6 we can move to a new scheme in which the \mathbf{r} are updated.

Rock physics model

A significant number of rock physics models have been developed, based on experimental data or physical theories or both, to relate the elastic properties of rock to porosity, mineralogy and pore fluid (Dvorkin, 2004). We examine a popular rock physics model: the stiff-sand model. This model is widely applied to clay-rich or shaly sandstones and even to shales (e.g., Spikes et al., 2007; Hossain et al., 2011; Grana, 2016; Wawrzyniak-Guz, 2019).

The stiff-sand model connects two end points in the elastic modulus versus porosity plane. The zero-porosity end point has the bulk and shear moduli of the solid phase K_0 and G_0 , which is calculated according to Voigt–Reuss–Hill average (Hill, 1952):

$$K_0 = \frac{1}{2} \left[\sum_{i=1}^N f_i K_i + \left(\sum_{i=1}^N f_i / K_i \right)^{-1} \right],$$

$$G_0 = \frac{1}{2} \left[\sum_{i=1}^N f_i G_i + \left(\sum_{i=1}^N f_i / G_i \right)^{-1} \right], \quad (7)$$

where N is the number of mineral components, f_i , K_i , and G_i are the volume fraction, bulk modulus, and shear modulus of the i th mineral component, respectively. Hertz-Mindlin grain-contact theory provides an estimation of the bulk and shear moduli of a dry rock, under the assumption that the rock frame is a random pack of spherical grains, subject to an effective pressure P_e , with a given porosity, and an average number of contacts per

grain n (coordination number). In the stiff sand model, Hertz-Mindlin equations are used to compute the bulk and shear moduli of the dry-rock K_{HM} and G_{HM} at the critical porosity ϕ_c :

$$K_{\text{HM}} = \left[\frac{n^2(1 - \phi_c)^2 G_0^2}{18\pi^2(1 - \nu_0)^2} P_e \right]^{1/3},$$

$$G_{\text{HM}} = \frac{2 + 3f - \nu_0(1 + 3f)}{5(2 - \nu_0)} \left[\frac{3n^2(1 - \phi_c)^2 G_0^2}{2\pi^2(1 - \nu_0)^2} P_e \right]^{1/3}, \quad (8)$$

where ν_0 is the Poisson's ratio of the solid phase, and f is the degree of adhesion between the grains. Then, for porosity $\phi \in (0, \phi_c)$, the bulk and shear moduli K_{dry} and G_{dry} of the dry-rock are estimated by interpolating the elastic moduli at zero porosity and at critical porosity using the modified Hashin-Shtrikman upper bounds:

$$K_{\text{dry}} = \left(\frac{\phi/\phi_c}{K_{\text{HM}} + 4/3G_0} + \frac{1 - \phi/\phi_c}{K_0 + 4/3G_0} \right)^{-1} - 4/3G_0,$$

$$G_{\text{dry}} = \left(\frac{\phi/\phi_c}{G_{\text{HM}} + \xi} + \frac{1 - \phi/\phi_c}{K_0 + \xi} \right)^{-1} - \xi, \quad (9)$$

where

$$\xi = \frac{G_0}{6} \frac{9K_0 + 8G_0}{K_0 + 2G_0}. \quad (10)$$

According to Gassmann's equations, the shear modulus of the saturated rock G_{sat} is the same as that of the dry rock, and the bulk modulus of the saturated rock K_{sat} is given by:

$$K_{\text{sat}} = K_{\text{dry}} + \frac{(1 - K_{\text{dry}}/K_0)^2}{\phi/K_f + (1 - \phi)/K_0 - K_{\text{dry}}/K_0^2}$$

where K_f is the bulk modulus of the fluid phase and is calculated using Reuss average:

$$K_f = \left(\sum_{i=1}^M f'_i / K'_i \right)^{-1}, \quad (11)$$

where M is the number of fluid components, f'_i and K'_i are the volume fraction and bulk modulus of the i th fluid component, respectively. The density of the saturated rock is computed as a weighted average of the densities of mineral and fluid components:

$$\rho = (1 - \phi) \sum_{i=1}^N f_i \rho_i + \phi \sum_{i=1}^M f'_i \rho'_i, \quad (12)$$

where ρ_i and ρ'_i are the density of the i th mineral component and the density of the i th fluid component, respectively. The velocities as functions of the elastic moduli and density are then

$$V_P = \sqrt{\frac{K_{\text{sat}} + \frac{4}{3}G_{\text{sat}}}{\rho}}, \quad V_S = \sqrt{\frac{G_{\text{sat}}}{\rho}}. \quad (13)$$

Table 1. Rock physics parameters used in this study

Parameter	Value	Parameter	Value
Quartz bulk modulus	37 GPa	CO ₂ bulk modulus	0.06 GPa
Quartz shear modulus	44 GPa	CO ₂ density	0.6 g/cm ³
Quartz density	2.65 g/cm ³	Effective pressure	10 MPa
Clay bulk modulus	16 GPa	Critical porosity	0.4
Clay shear modulus	9 GPa	Coordination number	9
Clay density	2.6 g/cm ³	Degree of adhesion	1
Water bulk modulus	2.2 GPa		
Water density	1.03 g/cm ³		

The partial derivatives of V_P , V_S , and ρ with respect to any rock physics parameters emerging from this model can be calculated using a mathematical software (e.g., MATLAB). We can then carry out FWI updates of these parameters according to equation 6.

In this study, we assume two mineral components, quartz and clay, and two fluid components, water and CO₂. Hence, we define three model unknowns: porosity (P), clay content (C) and CO₂ saturation (S_c). Additional rock physics parameters, including the elastic moduli and density of each mineral/fluid component, effective pressure, critical porosity, coordination number, and degree of adhesion between the grains, are fixed with the values in Table 1.

Rock physics FWI in the time lapse mode

CO₂ monitoring requires precise predictions of the CO₂ saturation model at any time at which the data are measured. Although it is possible to jointly invert the three parameters (porosity, clay content, and CO₂ saturation) from a single seismic survey, preliminary tests (including the work of Hu et al. (2021)) showed that fluid saturation is very difficult to estimate within this parameterization because of the large trade-off between rock physics parameters and its relatively small impact on the data. Here we consider a favorable case by making two assumptions: 1) before CO₂ injection, there is only one fluid component (water) in the subsurface; 2) Porosity and lithology parameters are constant in time. Therefore, we propose to estimate the three parameters sequentially: First, we apply the rock physics FWI approach as described earlier to the baseline (pre-injection) data for the estimation of porosity and clay content; then, we use the same inverse method and use the inverted porosity and clay content models from baseline survey as prior knowledge (fixed values) to estimate CO₂ saturation from monitor (post-injection) data. The objective function for baseline model reconstruction is expressed as

$$E_{baseline} = \|\mathbf{d}_{obs_b}(P^t, C^t, S_{c_b}^t = 0) - \mathbf{d}_{syn_b}(P, C, S_{c_b}^t = 0)\|^2, \quad (14)$$

where \mathbf{d}_{obs_b} and \mathbf{d}_{syn_b} denote the observed and synthetic baseline data, respectively. P^t and C^t denote the true porosity and clay content models. The baseline CO₂ saturation model $S_{c_b}^t$ is equal to 0 everywhere. The goal is to recovery the P and C models by iteratively minimizing the difference between \mathbf{d}_{obs_b} and \mathbf{d}_{syn_b} .

The objective function for monitor model reconstruction is

$$E_{\text{monitor}} = \|\mathbf{d}_{\text{obs}_m}(P^t, C^t, S_{c_m}^t) - \mathbf{d}_{\text{syn}_m}(P_{\text{inv}}, C_{\text{inv}}, S_{c_m})\|^2, \quad (15)$$

where $\mathbf{d}_{\text{obs}_m}$ and $\mathbf{d}_{\text{syn}_m}$ are the observed and synthetic monitor data, respectively. P_{inv} and C_{inv} are the inverted porosity and clay content models from baseline survey. They are used as input and will not be updated in the monitor model reconstruction. The goal is to recovery the saturation model S_{c_m} by iteratively minimizing the difference between $\mathbf{d}_{\text{obs}_m}$ and $\mathbf{d}_{\text{syn}_m}$.

NUMERICAL EXAMPLES

We apply the proposed approach to a CO₂ sequestration study based on the Johansen formation model. The Johansen formation is a deep saline aquifer and a candidate site for large-scale CO₂ storage offshore of the south-western coast of Norway. The geostatic model of the Johansen formation was built based on seismic and well-log data. Physical properties including porosity and permeability of this model are available (Eigestad et al., 2009). The original geo-cellular model is discretized in $100 \times 100 \times 5$ cells, however, we consider a vertical section through a sub-volume of cells centered around the injection well (FIG. 1a). The initial water saturation (before injection) is equal to 1 everywhere. The CO₂ saturation distribution in FIG. 1b is calculated by simulating the fluid flow in year 110, 10 years after stopping a 100-year injection (Grana et al., 2020).

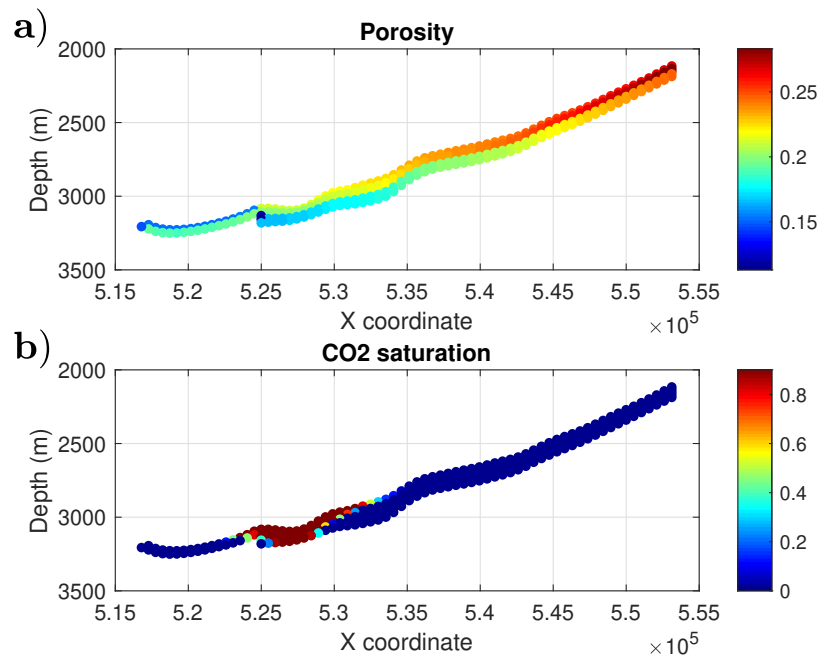


FIG. 1. True reservoir model of the Johansen formation: a) Porosity. b) CO₂ saturation distribution in year 110.

For numerical implementation of FWI, we make several changes to the model in FIG. 1. First, we define a regular grid and interpolate the scattered data over the grid. The grid consists of 76×81 node points with a depth increment of 20 m and a position increment of

500 m; second, we modify the coordinates by changing the starting depth to 0 m and the depth and position increments to 10 m. Moreover, to account for lithology in rock physics analysis, we introduce a clay volume with negative linear correlation with porosity. The reservoir models in FIG. 2 are then generated to examine the proposed FWI method.

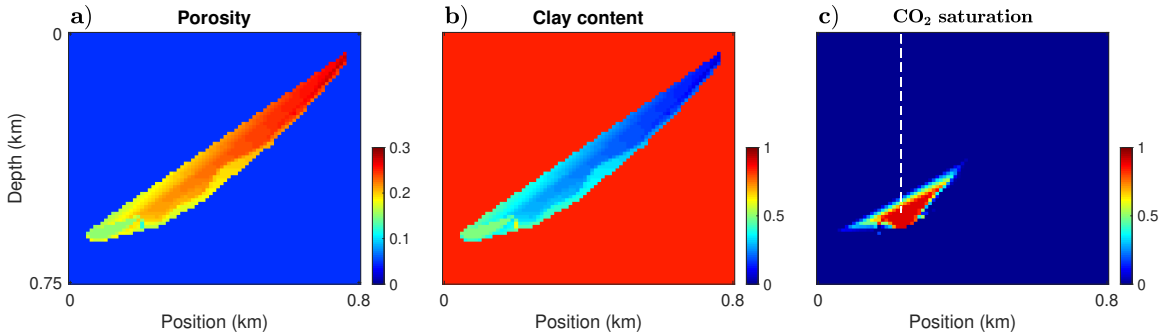


FIG. 2. True model of (a) porosity, (b) clay content, and (c) CO_2 saturation in year 110. White dashed line: Location of the injection well.

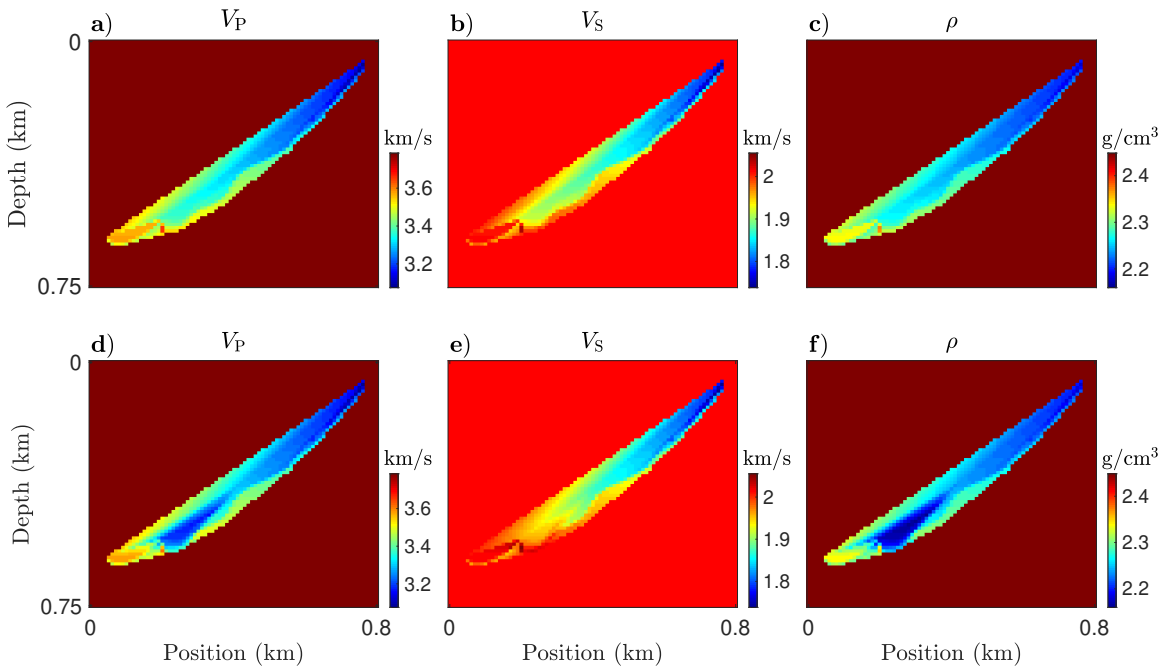


FIG. 3. True model of P- and S-wave velocities plus density. (a-c) Baseline. (d-f) Monitor.

The sandstone reservoir is distinguished by higher porosity and lower clay content values compared to the surrounding shale. Porosity in the sand layers varies between 0.15 and 0.29, with the porosity within a zone degrading towards south as the depth of the formation increases. The shale layers have a constant porosity of 0.05 and clay content of 0.85. The initial CO_2 saturation model is equal to 0 everywhere and then changes locally due to the injection. In FIG. 3, the velocity and density models calculated by rock physics modeling are plotted. With CO_2 replacing water, the density of the saturated rock decreases due to the lower density of CO_2 , the P-wave velocity decreases due to the lower bulk modulus of

CO₂, and the S-wave velocity slightly increases since the fluid only affects the density in the S-wave velocity expression.

The inversion experiments are presented in two parts: first, we estimate the porosity and clay content models from baseline seismic survey; then, we use the inverted porosity and clay content models as input in the monitor stage to estimate CO₂ saturation distribution. In these experiments, the data are computed with the same algorithm for observed and synthetic data in inversion. We adopt a multiscale approach (Bunks et al., 1995) by inverting multiple frequency bands, each containing five evenly spaced frequencies from 2 Hz to a maximum frequency; the maximum frequency is 3 Hz for the first band, and it increases to 25 Hz for the last band. A TGN optimization method, comprising 20 inner iterations and 1 outer iteration for each frequency band, is used. We use an acquisition geometry with receivers mimicking a simultaneous surface seismic and vertical seismic profile configuration: a line of sources every 50 m at the top of the model illuminates receivers every 20 m on the top and sides of the model.

Baseline model reconstruction

One of the challenges of predicting rock physics properties from seismic data is the low frequency (initial) model. In a typical elastic inversion, the low frequency model of velocity is often related to models used for seismic processing, for example stacking velocities. In the rock physics domain, a low frequency model is harder to define because different lithologies might have different rock physics models. Here we examine three initial models which are realistic in terms of assumptions of what we know:

- (1) We subsample the true model (assuming core or well log data are available) and interpolate on the original grid to lose the frequency. 12 samples of the reservoir layer are used for interpolation;
- (2) We filter the true model of velocity (Figure 3a) and apply a linear regression for porosity. The true velocity-porosity relationship is not linear, but the nonlinearity is not strong;
- (3) We assume exact horizons are available and we set constant rock physics properties in each layer. A constant porosity of 0.2 and clay content of 0.3 are assigned to the reservoir layer.

The initial porosity models built by these means, which we call "subsample", "regression", and "constant" for short, are plotted in FIG. 4a-c. The initial clay content models (FIG. 4d-f) are computed from porosity based on the exact relationship between them.

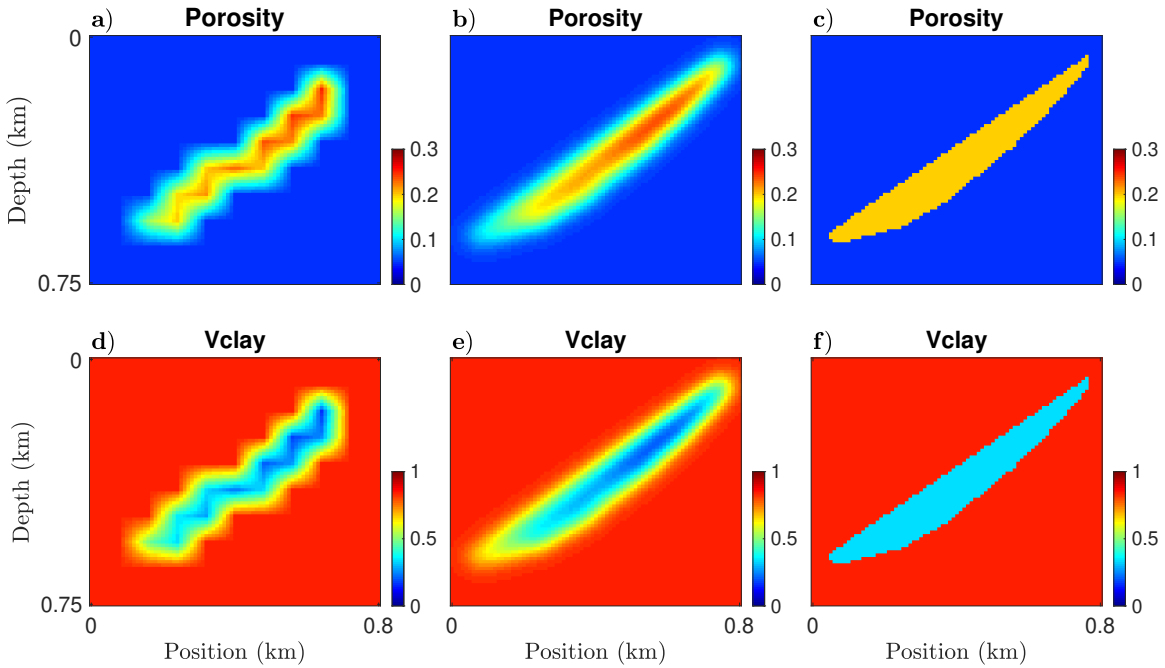


FIG. 4. Initial porosity and clay content models: (a and b) subsample, (b and e) regression, and (c and f) constant.

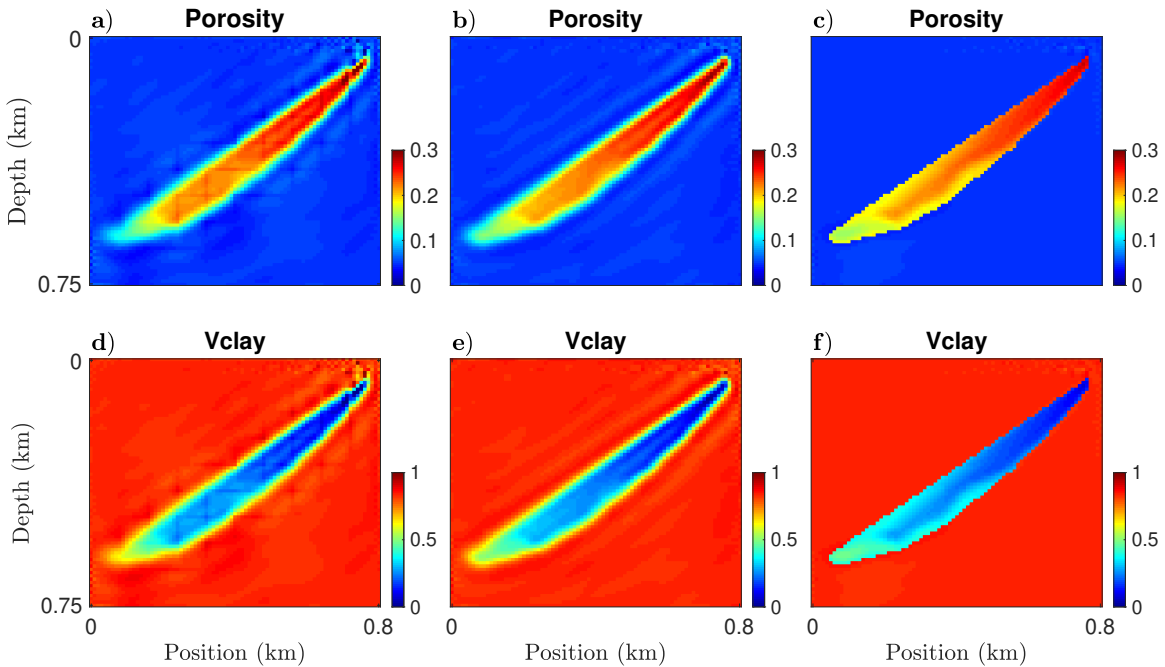


FIG. 5. Baseline model reconstruction with noise-free data. Inverted porosity and clay content models starting from different initial models. (a and d) Subsample, (b and e) regression, and (c and f) constant.

We first perform the investigation with noise-free data. We adopt the regularization strategy of Hu and Innanen (2021) to enforce explicit physical relationships between the updated parameters. FIG. 5 shows that the porosity and clay content models can be well

resolved using any of the three initial models. However, the “constant” initial model leads to the best result, with the structure and parameter values of the model perfectly estimated. The result with the “subsample” initial model appears to fare the worst, containing some footprint of the initial model. This observation is confirmed by comparing their vertical profiles (FIG. 6a). In FIG. 6b, the error reduction history associated with the three initial models is plotted. The model error is computed as the 2-norm of the difference between the updated and true models. We observe that the “constant” initial model has very small errors, as compared to the other two, and this appears to be an important factor contributing to its superiority in the final result. The “subsample” initial model is least accurate, however, its errors decrease most rapidly and eventually get very close to that of the “regression” model. This illustrates that different versions of smooth initial model may lead to very similar inversion results.

The results with noisy data remain consistent with the noise-free test: the porosity and clay content models are still accurately recovered, even though more noisy. This confirms the robustness of our approach for baseline model reconstruction. Although the “constant” initial model leads to the best estimates, assuming exact horizons are known is greedy. Therefore, we choose the result of the more realistic, smooth initial model in the monitor survey to estimate CO₂ saturation.

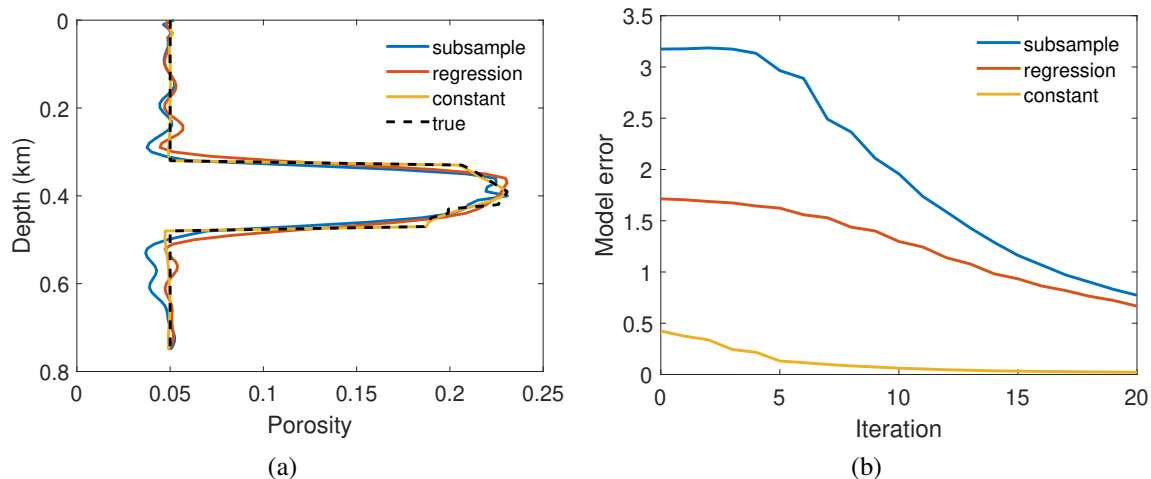


FIG. 6. Comparison between the inverted porosity models in FIG. 5. (a) Model profiles at a lateral position of 0.4 km and (b) model error reductions.

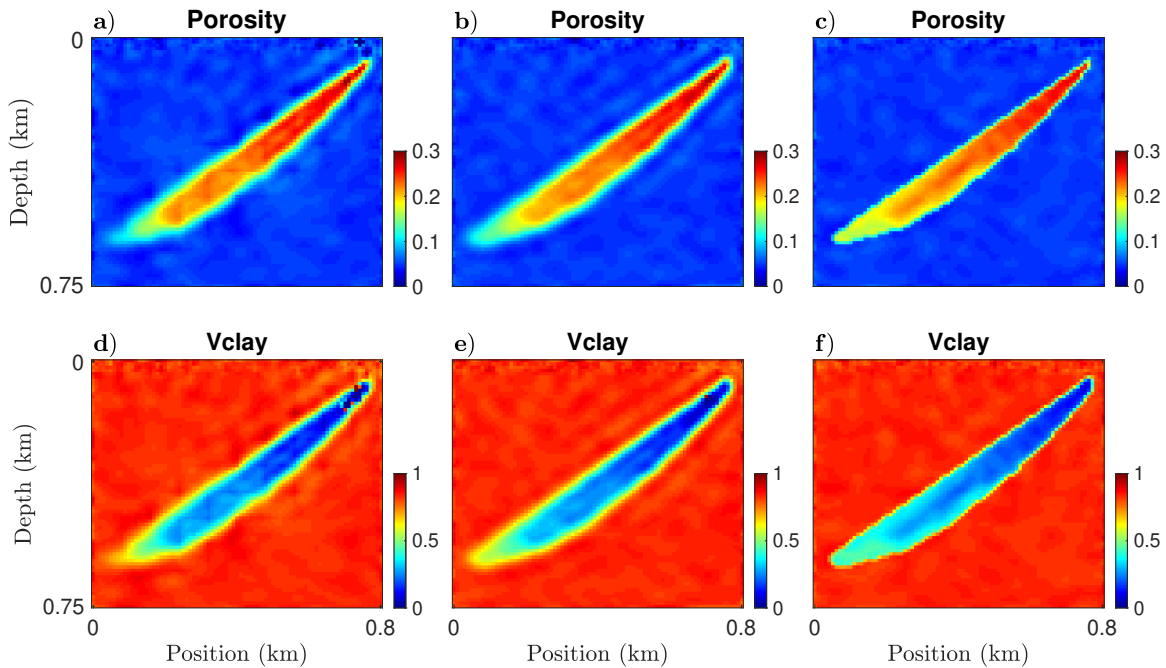


FIG. 7. Baseline model reconstruction with noisy data (SNR=10). Inverted porosity and clay content models starting from different initial models. (a and d) Subsample, (b and e) regression, and (c and f) constant.

Monitor model reconstruction

In the monitor survey, the observed data is generated from the true porosity, clay content, and CO_2 saturation models in FIG.2; the synthetic data is generated from the porosity and clay content estimated from baseline data plus the current estimate of CO_2 saturation. If uncertainty in the monitor data is considered, there are two factors that could have a negative impact on the CO_2 estimation: errors in the baseline model estimates and errors in the monitor data.

We first carry out noise-free tests to examine the impact of baseline model estimates. Three cases are considered: the baseline model is poorly, properly, and perfectly resolved. For this, we use the smooth initial model in FIG. 4b and 4e, the inverted model in FIG. 7b and 7e, and the true model in FIG. 2a and 2b, respectively, as input. FIG. 8d-f shows the recovered CO_2 saturation models in these cases. For the case of poorly constructed baseline model, we can clearly observe the effect known as parameter crosstalk, which arises from the complex manner in which multiple subsurface properties co-determine seismic waveforms, and occurs when errors in one property are mapped into the updates of another. As a result, the recovered CO_2 saturation model is highly contaminated by the errors in porosity and clay content estimates. With properly reconstructed baseline model, the CO_2 saturation is recovered to some extent, with the shape of the plume slightly distorted and the parameter values slightly overestimated. Crosstalk artifacts still exist, especially in the near surface area and the upper right section of the reservoir. These errors in the CO_2 estimates can be interpreted as a consequence of erroneous baseline model input, if using the case of perfect baseline model, in which the CO_2 model is accurately recovered, as a reference.

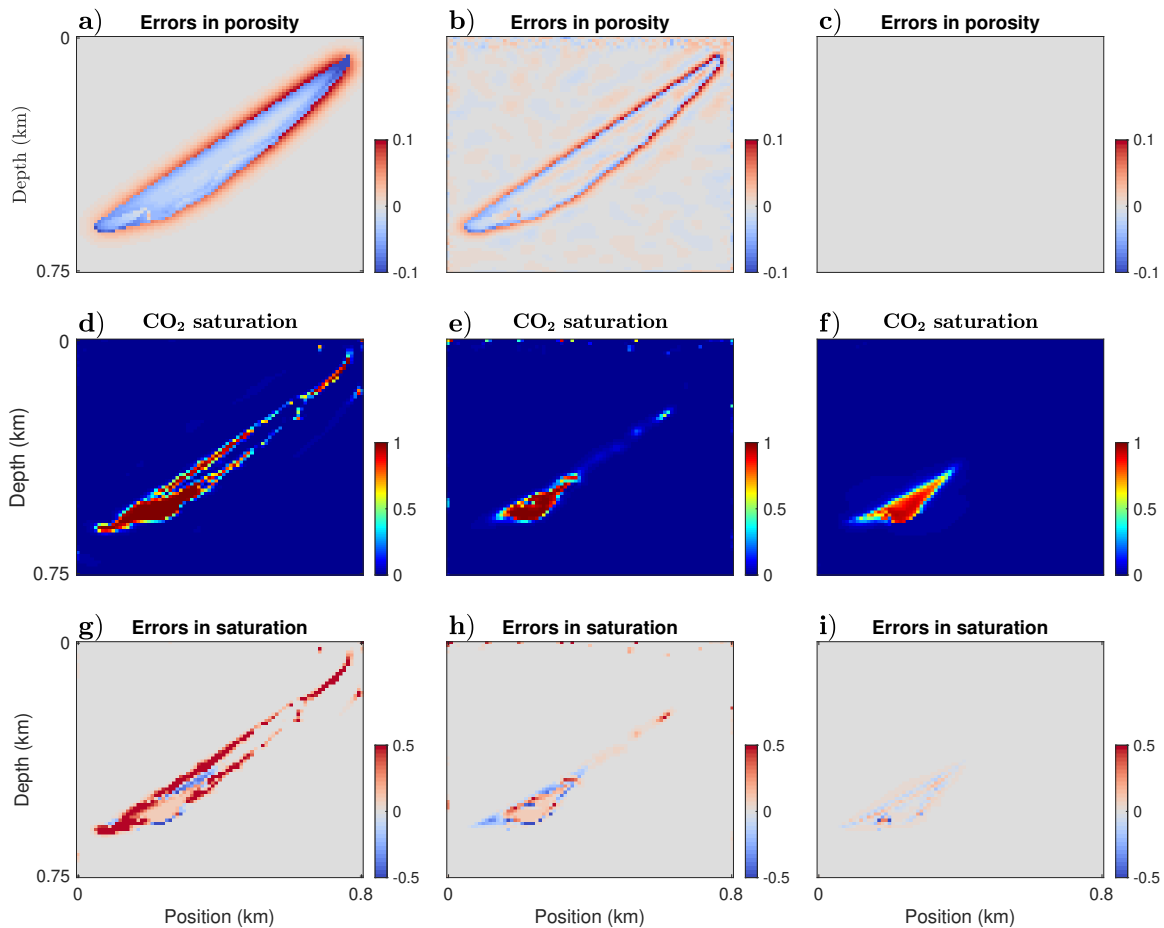


FIG. 8. Inversion test to examine the impact of the errors in baseline model estimates on monitor model reconstruction, using noise-free monitor data. Three baseline models are used as input: the initial model in FIG. 4b and 4e, the inverted model in FIG. 7b and 7e, and the true model in FIG. 2a and 2b. (a-c) Errors in the initial, inverted, and true porosity models, and (d-f) the resulting CO₂ saturation estimates and (g-i) their errors.

Next we use the inverted baseline models in FIG. 7b and 7e as input and examine the random noise effects. We add random Gaussian noise to the true noise-free data considering three noise levels: signal-to-noise ratio (SNR) are 20, 10, and 5. In FIG. 9, we observe that compared to the result of noise-free data (FIG. 8e), the inverted models are contaminated by artifacts more seriously. Most of all, with moderate and strong noise levels (SNR=10 and 5), the distribution of CO₂ saturation becomes patchy and the plume covers the entire reservoir area.

Since CO₂ saturation is the only variable in monitor model reconstruction, the errors in the baseline model estimates will amount to errors in the monitor data. Therefore, we can interpret the poor result in FIG. 9 as a consequence of errors in the data. Furthermore, we can say that the estimation of CO₂ saturation from monitor data is an ill-conditioned problem because the solution is sensitive to errors in the data. The basic idea in the treatment of ill-conditioned problems is to use some prior information about solutions to disqualify meaningless ones. This can be achieved using the technique known as regularization, which involves modification of the objective function by adding a model penalty term.

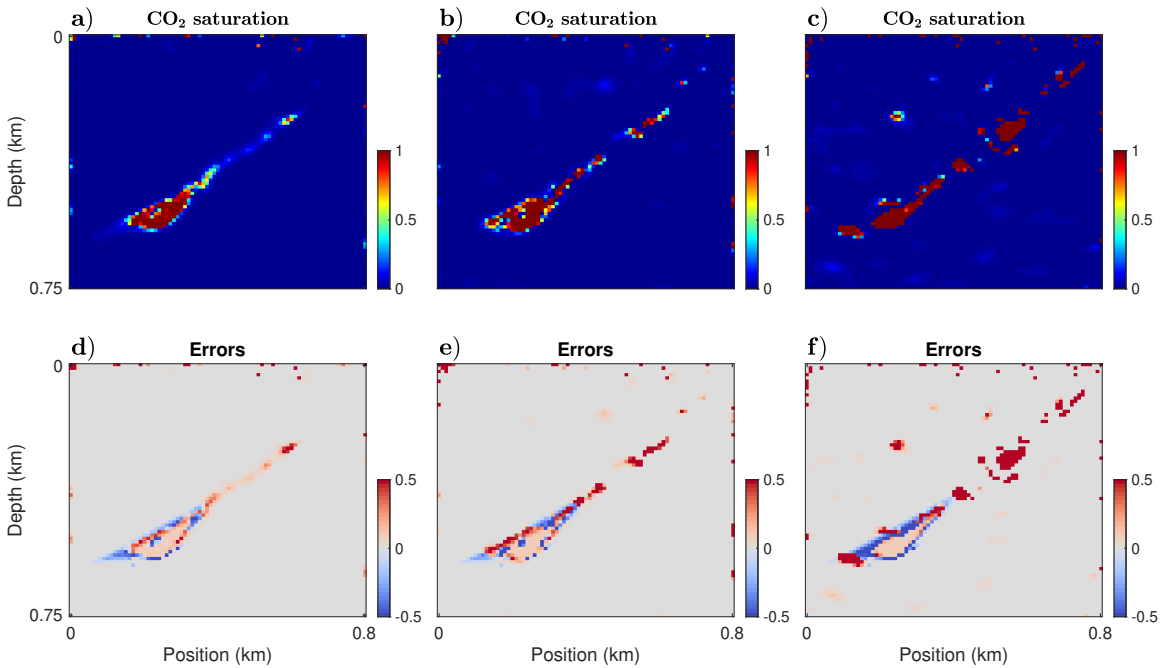


FIG. 9. Inversion test to examine the impact of errors in monitor data. The inverted porosity and clay content models in FIG. 7b and 7e are used as input. (a-c) Recovered CO₂ saturation models with a signal-to-noise ratio of 20, 10, and 5, respectively, and (d-f) their corresponding errors.

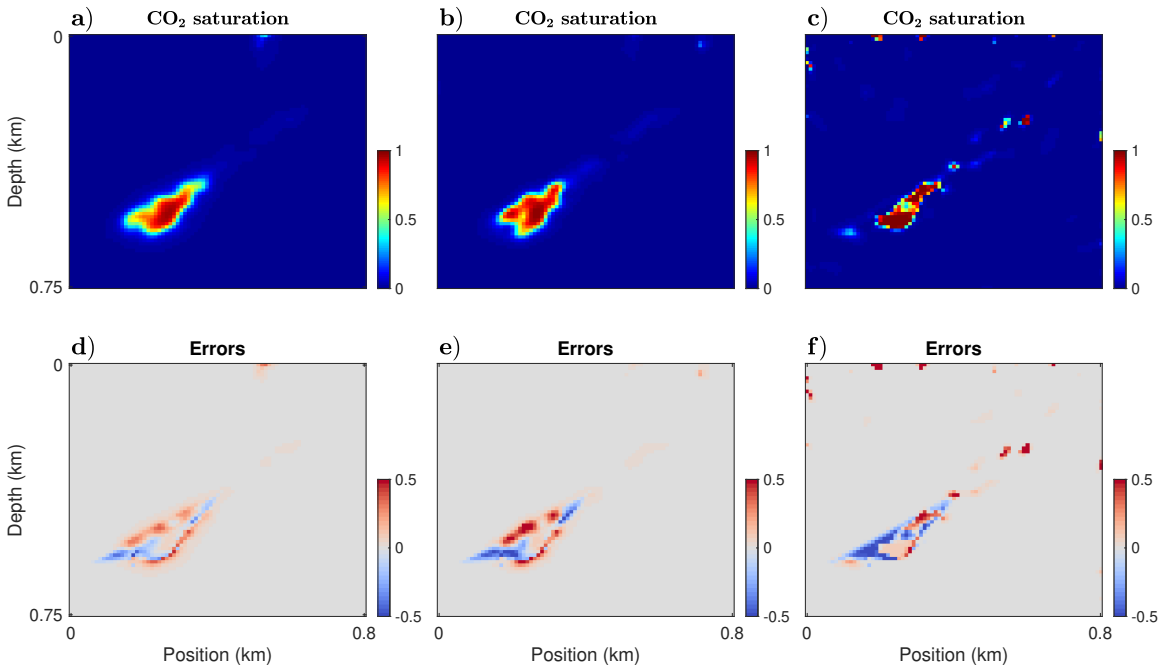


FIG. 10. Repeat the inversion test in FIG.9 using regularization technique to impose smoothness on the model. (a-c) Recovered CO₂ saturation models with a signal-to-noise ratio of 20, 10, and 5, respectively, and (d-f) their corresponding errors.

We first consider the First-order Tikhonov regularization (Tikhonov and Arsenin, 1977). This regularization scheme is based on the assumption that neighboring points in the model should be close in value, leading to smooth solutions. The results are plotted in FIG. 10. Compared to the result in FIG. 9, the sparsely distributed artifacts are effectively reduced and the continuity in the distribution of CO₂ is preserved, leading to an estimate that matches more closely the true model. However, this regularization causes an attenuation of the high wavenumbers present in the model.

In many instances we may have a very good reference (or prior) model. Thus in the inversion, in addition to minimizing the misfit between observed and synthetic data, we impose the restriction that the model does not deviate much from the prior model. This can be done by adding a prior model term to the objective function (Sen and Roy, 2003). For the Johansen model case, it is realistic to assume that CO₂ has the highest accumulation at the injection well and then decreases as the distance from the well increases. We build a prior model assuming that the CO₂ plume has migrated 20 traces to the left and 20 traces to the right, within the reservoir, at the time the monitor data were acquired (FIG. 11c). The inversion results with this prior model constraint are plotted in FIG. 12. We see that the prior model term helps to restrict the model updates within the deeper part of the model, thus largely reducing the artifacts in the upper right area (FIG. 9). However, the result remains contaminated by the footprint of the prior model, and the continuity of the CO₂ plume is not guaranteed.

We consequently include both the Tikhonov term and prior model term in the objective function, to encourage smoothness, and at the same to keep the inverted model from deviating significantly from the prior model. The result shows a better agreement with the true model compared to any of the results described earlier.

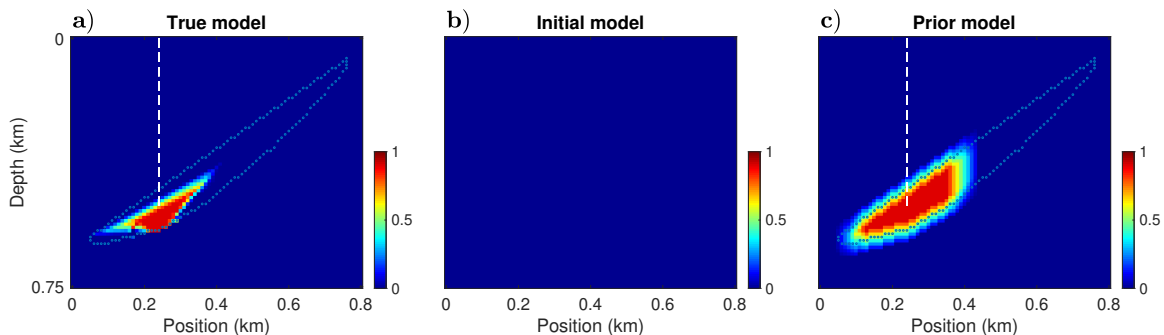


FIG. 11. (a-c) True model, initial model, and prior model, respectively. The white dashed line denotes the location of the injection well. The blue dashed line denotes the boundary of the sandstone reservoir. The prior model is built upon the assumption that the CO₂ plume has migrated 20 traces to the left and 20 traces to the right, within the reservoir, at the time the monitor data were acquired.

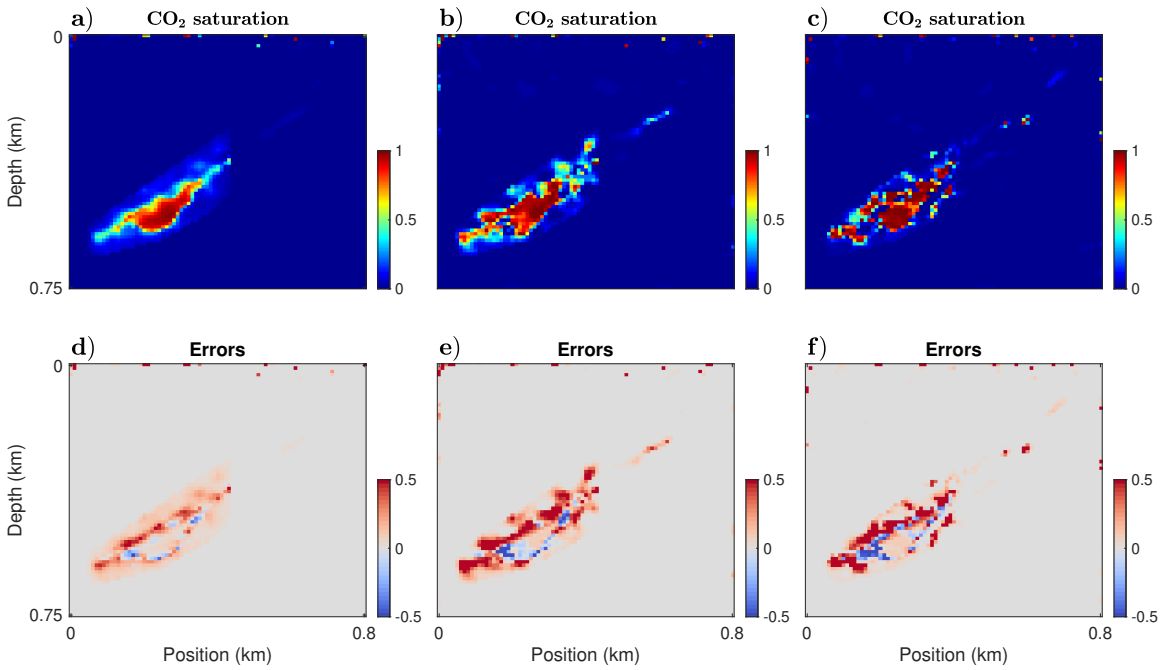


FIG. 12. Repeat the inversion test in FIG.9 using prior model constraint. (a-c) Recovered CO₂ saturation models with a signal-to-noise ratio of 20, 10, and 5, respectively, and (d-f) their corresponding errors.

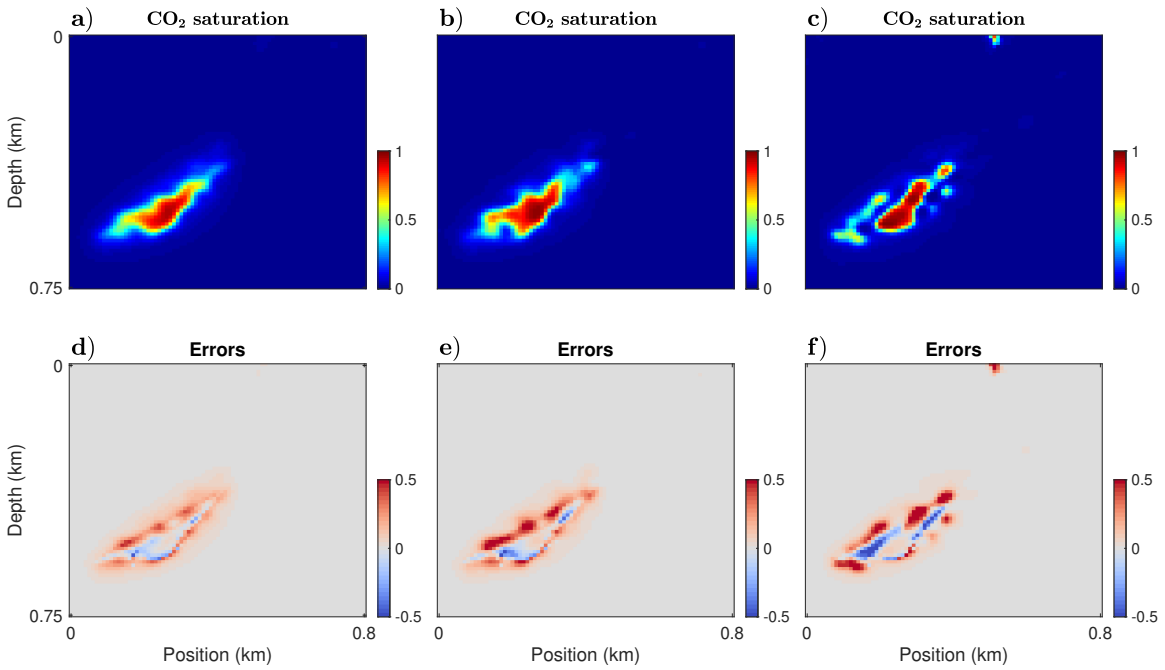


FIG. 13. Repeat the inversion test in FIG.9 using both smoothness and prior model constraints. (a-c) Recovered CO₂ saturation models with a signal-to-noise ratio of 20, 10, and 5, respectively, and (d-f) their corresponding errors.

CONCLUSIONS

We presented a full waveform inversion method for the prediction of rock and fluid properties, namely, porosity, lithology and time-dependent CO₂ saturation values from seismic data. The method was validated on synthetic data generated for the Johansen formation model. We derive porosity and lithology parameters from baseline data and use them as input to obtain 2D spatial distribution of CO₂ saturation from monitor data. The CO₂ recovery can be seriously contaminated by the artifacts that arise from errors in the baseline models and random noise in the monitor data. In this case, we show that imposing model constraints can significantly improve the result.

ACKNOWLEDGMENTS

We thank the sponsors of CREWES for continued support. This work was funded by CREWES industrial sponsors and NSERC (Natural Science and Engineering Research Council of Canada) through the grant CRDPJ 543578-19. The first author was partially supported by a scholarship from the SEG Foundation.

REFERENCES

- Alemie, W. M., 2017, Time-lapse full waveform inversion methods: Ph.D. thesis.
- Asnaashari, A., Brossier, R., Garambois, S., Audebert, F., Thore, P., and Virieux, J., 2015, Time-lapse seismic imaging using regularized full-waveform inversion with a prior model: which strategy?: *Geophysical prospecting*, **63**, No. 1, 78–98.
- Bosch, M., Cara, L., Rodrigues, J., Navarro, A., and Díaz, M., 2007, A monte carlo approach to the joint estimation of reservoir and elastic parameters from seismic amplitudes: *Geophysics*, **72**, No. 6, O29–O39.
- Bosch, M., Mukerji, T., and Gonzalez, E. F., 2010, Seismic inversion for reservoir properties combining statistical rock physics and geostatistics: A review: *Geophysics*, **75**, No. 5, 75A165–75A176.
- Brossier, R., Operto, S., and Virieux, J., 2009, Seismic imaging of complex onshore structures by 2D elastic frequency-domain full-waveform inversion: *Geophysics*, **74**, No. 6, WCC105–WCC118.
- De Barros, L., and Dietrich, M., 2008, Perturbations of the seismic reflectivity of a fluid-saturated depth-dependent poroelastic medium: *The Journal of the Acoustical Society of America*, **123**, No. 3, 1409–1420.
- Doyen, P., 2007, *Seismic reservoir characterization: An earth modelling perspective*: EAGE publications.
- Dupuy, B., Romdhane, A., Eliasson, P., and Yan, H., 2021, Combined geophysical and rock physics workflow for quantitative co2 monitoring: *International Journal of Greenhouse Gas Control*, **106**, 103,217.
- Dvorkin, J., 2004, Seismic reflections of rock properties: *Hart's E & P*, **77**, No. 11, 59–61.

- Eigestad, G. T., Dahle, H. K., Hellevang, B., Riis, F., Johansen, W. T., and Øian, E., 2009, Geological modeling and simulation of co₂ injection in the johansen formation: *Computational Geosciences*, **13**, No. 4, 435.
- Fu, X., Romahn, S., and Innanen, K., 2020, Double-wavelet double-difference time-lapse waveform inversion, *in* SEG Technical Program Expanded Abstracts 2020, Society of Exploration Geophysicists, 3764–3767.
- Ghosh, R., Sen, M. K., and Vedanti, N., 2015, Quantitative interpretation of co₂ plume from sleipner (north sea), using post-stack inversion and rock physics modeling: *International journal of greenhouse gas control*, **32**, 147–158.
- Grana, D., 2016, Bayesian linearized rock-physics inversion: *Geophysics*, **81**, No. 6, D625–D641.
- Grana, D., Liu, M., and Ayani, M., 2020, Prediction of CO₂ saturation spatial distribution using geostatistical inversion of time-lapse geophysical data: *IEEE Transactions on Geoscience and Remote Sensing*.
- Grude, S., Landrø, M., and Osdal, B., 2013, Time-lapse pressure–saturation discrimination for co₂ storage at the snøhvit field: *International Journal of Greenhouse Gas Control*, **19**, 369–378.
- Hill, R., 1952, The elastic behaviour of a crystalline aggregate: *Proceedings of the Physical Society. Section A*, **65**, No. 5, 349.
- Hossain, Z., Mukerji, T., Dvorkin, J., and Fabricius, I. L., 2011, Rock physics model of glauconitic greensand from the north sea: *Geophysics*, **76**, No. 6, E199–E209.
- Hu, Q., and Innanen, K., 2021, Elastic full-waveform inversion with rock-physics constraints, *in* First International Meeting for Applied Geoscience & Energy, Society of Exploration Geophysicists, 662–666.
- Hu, Q., Keating, S., Innanen, K. A., and Chen, H., 2021, Direct updating of rock-physics properties using elastic full-waveform inversion: *Geophysics*, **86**, No. 3, MR117–MR132.
- Kamei, R., and Lumley, D., 2017, Full waveform inversion of repeating seismic events to estimate time-lapse velocity changes: *Geophysical Journal International*, **209**, No. 2, 1239–1264.
- Liu, M., and Grana, D., 2018, Stochastic nonlinear inversion of seismic data for the estimation of petroelastic properties using the ensemble smoother and data reparameterization: *Geophysics*, **83**, No. 3, M25–M39.
- Macquet, M., Lawton, D. C., Saeedfar, A., and Osadetz, K. G., 2019, A feasibility study for detection thresholds of co₂ at shallow depths at the cami field research station, newell county, alberta, canada: *Petroleum Geoscience*, **25**, No. 4, 509–518.

- Mallick, S., and Adhikari, S., 2015, Amplitude-variation-with-offset and prestack-waveform inversion: A direct comparison using a real data example from the rock springs uplift, Wyoming, USA: *Geophysics*, **80**, No. 2, B45–B59.
- Mavko, G., Mukerji, T., and Dvorkin, J., 2009, *The rock physics handbook: Tools for seismic analysis of porous media*: Cambridge University Press.
- Métivier, L., Brossier, R., Operto, S., and Virieux, J., 2017, Full waveform inversion and the truncated Newton method: *SIAM Review*, **59**, No. 1, 153–195.
- Morency, C., Luo, Y., and Tromp, J., 2009, Finite-frequency kernels for wave propagation in porous media based upon adjoint methods: *Geophysical Journal International*, **179**, No. 2, 1148–1168.
- Operto, S., Gholami, Y., Prieux, V., Ribodetti, A., Brossier, R., Metivier, L., and Virieux, J., 2013, A guided tour of multiparameter full-waveform inversion with multicomponent data: From theory to practice: *The Leading Edge*, **32**, No. 9, 1040–1054.
- Pan, W. Y., Innanen, K. A., Geng, Y., and Li, J. X., 2019, Interparameter trade-off quantification for isotropic-elastic full-waveform inversion with various model parameterizations: *Geophysics*, **84**, No. 2, R185–R206.
- Pratt, R. G., 1990, Frequency-domain elastic wave modeling by finite differences: A tool for crosshole seismic imaging: *Geophysics*, **55**, No. 5, 626–632.
- Prieux, V., Brossier, R., Operto, S., and Virieux, J., 2013, Multiparameter full waveform inversion of multicomponent ocean-bottom-cable data from the Valhall field. Part 1: Imaging compressional wave speed, density and attenuation: *Geophysical Journal International*, **194**, No. 3, 1640–1664.
- Queißer, M., and Singh, S. C., 2013a, Full waveform inversion in the time lapse mode applied to co2 storage at sleipner: *Geophysical prospecting*, **61**, No. 3, 537–555.
- Queißer, M., and Singh, S. C., 2013b, Localizing co 2 at sleipner—seismic images versus p-wave velocities from waveform inversion: *Geophysics*, **78**, No. 3, B131–B146.
- Roach, L. A., White, D. J., and Roberts, B., 2015, Assessment of 4d seismic repeatability and co2 detection limits using a sparse permanent land array at the aquistore co2 storage site: *Geophysics*, **80**, No. 2, WA1–WA13.
- Russell, B. H., Gray, D., and Hampson, D. P., 2011, Linearized AVO and poroelasticity: *Geophysics*, **76**, No. 3, C19–C29.
- Sen, M. K., and Roy, I. G., 2003, Computation of differential seismograms and iteration adaptive regularization in prestack waveform inversion: *Geophysics*, **68**, No. 6, 2026–2039.
- Shulakova, V., Pevzner, R., Dupuis, J. C., Urosevic, M., Tertyshnikov, K., Lumley, D. E., and Gurevich, B., 2015, Burying receivers for improved time-lapse seismic repeatability: Co2crc otway field experiment: *Geophysical Prospecting*, **63**, No. 1, 55–69.

- Spikes, K., Mukerji, T., Dvorkin, J., and Mavko, G., 2007, Probabilistic seismic inversion based on rock-physics models: *Geophysics*, **72**, No. 5, R87–R97.
- Tarantola, A., 1986, A strategy for nonlinear elastic inversion of seismic reflection data: *Geophysics*, **51**, No. 10, 1893–1903.
- Tikhonov, A. N., and Arsenin, V. Y., 1977, *Solutions of ill-posed problems*: Winston and Sons.
- Virieux, J., and Operto, S., 2009, An overview of full-waveform inversion in exploration geophysics: *Geophysics*, **74**, No. 6, WCC1–WCC26.
- Wawrzyniak-Guz, K., 2019, Rock physics modelling for determination of effective elastic properties of the lower Paleozoic shale formation, North Poland: *Acta Geophysica*, **67**, No. 6, 1967–1989.
- Yang, Q., Malcolm, A., Rusmanugroho, H., and Mao, W., 2019, Analysis of radiation patterns for optimized full waveform inversion in fluid-saturated porous media: *Geophysical Journal International*, **216**, No. 3, 1919–1937.